AIAA JOURNAL
Vol. 45, No. 1, January 2007

Aerodynamics of a NACA4412 Airfoil in Ground Effect

M. R. Ahmed*
The University of the South Pacific, Suva, Fiji
and
T. Takasaki† and Y. Kohama‡
Tohoku University, Sendai 980-8577, Japan

DOI: 10.2514/1.23872

The flow characteristics over a NACA4412 airfoil are studied in a low turbulence wind tunnel with moving ground simulation at a Reynolds number of 3.0×10^5 by varying the angle of attack from 0 to 10 deg and ground clearance of the trailing edge from 5% of chord to 100%. The pressure distribution on the airfoil surface was obtained, velocity survey over the surface was performed, wake region was explored, and lift and drag forces were measured. To ensure that the flow is 2-D, particle image velocimetry measurements were performed. A strong suction effect on the lower surface at an angle of attack of 0 deg at the smallest ground clearance caused laminar separation well ahead of the trailing edge. Interestingly, for this airfoil, a loss of upper surface suction was recorded as the airfoil approached the ground for all angles of attack. For angles up to 4 deg, the lift decreased with reducing ground clearance, whereas for higher angles, it increased due to a higher pressure on the lower surface. The drag was higher close to the ground for all angles investigated mainly due to the modification of the lower surface pressure distribution.

Nomenclature

A	=	area of the airfoil ($c \times$ span)
C_d	=	coefficient of drag ($D/0.5\rho A U_\infty^2$)
C_l	=	coefficient of lift ($L/0.5\rho A U_\infty^2$)
C_p	=	coefficient of pressure ($[p - p_\infty]/0.5\rho U_\infty^2$)
c	=	chord length of the airfoil
D	=	drag force
h	=	height of trailing edge above the ground
L	=	lift force
l	=	streamwise distance from the trailing edge
p	=	static pressure
p_∞	=	freestream static pressure
Re	=	Reynolds number
U_∞	=	freestream mean velocity
u	=	streamwise mean velocity at a point
$\sqrt{\overline{u'^2}}$	=	rms value of the fluctuations in u
x	=	distance from the leading edge (along the chord)
y	=	transverse (spanwise) coordinate
z	=	vertical coordinate (measured from the airfoil surface)
z'	=	vertical coordinate (measured from the ground)
α	=	angle of attack
ρ	=	air density

I. Introduction

THE flow around an airfoil is considerably modified under the influence of ground effect. The dividing streamline and the stagnation point generally move down for positive angles of attack, causing a reduction in velocity and an increase in pressure under the airfoil. This results in the buildup of a high pressure under the airfoil, creating an air cushion. For very small clearances, the air tends to stagnate under the airfoil, which gives the highest possible pressure, called ram pressure. Most of the airfoils generate a higher lift close to the ground at moderate angles of attack due to the higher pressure on the lower surface. For some airfoil geometries, the suction on the upper surface gets enhanced due to divergence of the flow towards the upper surface, further increasing the lift. The pressure drag may decrease with reducing ground clearance if there is a higher contribution of the modified upper surface suction in the direction opposite to that of drag; otherwise the pressure drag is higher at low ground clearances due to the higher contribution to the pressure drag mainly from the lower surface. The skin friction drag also changes in close ground proximity due to significant changes in the velocities on both the sides of the airfoil. The streamline patterns over the leading and trailing edges of an airfoil in ground effect can be seen in [1].

The induced drag for a three-dimensional wing reduces close to the ground as the streamlines are forced to become parallel to the ground causing the downwash to diminish. This normally results in a reduction in total drag. The increased lift and reduced drag obtained for a wing-in-ground-effect (WIG) vehicle result in a much higher efficiency, which helps to increase the flight range at a reduced specific fuel consumption compared with the conventional aircraft. The L/D value is a measure of the efficiency [2], because thrust is equal to drag and weight is equal to lift in steady flight. Works on development of WIG vehicles can benefit immensely if the advantages of ground proximity are fully used. Development of WIG vehicles of different sizes requires aerodynamic data over a wide range of Reynolds numbers. Apart from seaplanes and small WIG vehicles, the results from the present work, carried out at $Re = 3 \times 10^5$, will be applicable to sailplanes, human-powered vehicles, unmanned air vehicles (UAVs) and micro-air vehicles (MAVs) that operate in ground effect. Moreover, the rapidly increasing capabilities of CFD give rise to the need of extensive experimental data that can be used for validation of numerical codes which can later be extended to different flow conditions.

II. Background

The effects of proximity to ground for an airfoil on the lift and drag characteristics were studied as early as in 1920s [3,4]. A review of the various types of WIG vehicles experimented at various times is made by Ollila [5]. There have been experimental as well as numerical studies on the influence of ground proximity on the aerodynamic characteristics of different airfoil configurations [6–31]. Most of the experimental and numerical studies carried out on regular airfoils in

Presented as Paper 258 at the 44th Aerospace Sciences Meeting & Exhibit, Reno, NV, 9–12 January 2006; received 13 March 2006; revision received 2 June 2006; accepted for publication 5 June 2006.

*Senior Lecturer, School of Engineering, Laucala Campus. Senior Member AIAA.
†Graduate Student, Low Turbulence Wind Tunnel Laboratory, Institute of Fluid Science, 2-1-1 Katahira. Non-Member AIAA.
‡Professor, Low Turbulence Wind Tunnel Laboratory, Institute of Fluid Science, 2-1-1 Katahira. Non-Member AIAA.

context of WIG vehicles [6–24] reported an increase in lift when an airfoil is run close to the ground. Measurements were performed by Fink and Lastinger [6] at $Re = 4.9 \times 10^5$ on a Glenn Martin 21 airfoil (that was modified to provide a flat bottom from $0.3c$ to the trailing edge) at $\alpha = -10$–20 deg and $h/c = 0.046$–1.0 to evaluate the ground effect for aspect ratios of 1–6 using the image-wing method. Staufenbiel et al. [7] did numerical calculations based on surface singularity method and performed experiments with a fixed ground plate equipped with a suction system on a 11.7% thick Clark-Y airfoil at $\alpha = 3$–6 deg and $h/c = 0.05$ at $Re = 1.3 \times 10^6$. Fuwa et al. [8] in their work on rectangular NACA6409 wings with a rounded edge and with a flat end-plate (aspect ratio 0.6) in a towing tank varied h/c from 0.01 to 0.5 and found that C_l and C_d are higher close to the ground for $\alpha = 6$ deg. They also performed a detailed safety assessment of WIG vehicles. Chawla et al. [9] studied the WIG phenomenon for a NACA4415 wing having an aspect ratio of 2.33 with and without end-plates using a fixed ground plate. The angle of attack was varied from 0 to 25 deg and h/c (h was measured at $c/4$) from 0.25 to 2.35. They found that the end-plates significantly improved C_l for low h. Tomaru and Kohama [10] conducted experiments on NACA6412 and NACA23012 airfoils (end-plates were used with wings of aspect ratio 4) with fixed ground plates at $Re = 4.0 \times 10^5$, $\alpha = 0$–12.5 deg and $h/c = 0.05$–1.0. They reported generally increasing C_l values and decreasing C_d values as the ground is approached except for a few cases of $\alpha = 0$ and 2.5 deg; that will be discussed later. They also conducted experiments on NACA0012-64 and reported some interesting results. Hsiun and Chen [11] investigated the aerodynamic characteristics of NACA4412 airfoil with ground effect in viscous flow through the use of numerical method by varying Re from 2×10^5 to 2×10^6 and h/c from 0.05 to 1.0 at $\alpha = 5$ and 10 deg with a fixed ground plate. Coulliette and Plotkin [12] obtained pressure distribution and estimated C_l numerically and analytically on flat plate, parabolic arc, and symmetrical Joukowski airfoils with different cambers and thicknesses using inviscid flow equations; the ground clearance was varied from $h/c = 0$ to 1.5 and α from 0 to 15 deg. Detailed measurements of C_l and C_d for a 9% thick cambered airfoil were performed by Chun et al. [14] for aspect ratios of 1 and 2. They found increasing C_l and decreasing C_d values as the ground is approached for the higher aspect ratio of 2 for values of α ranging from 0 to 8 deg. It was also found that for the aspect ratio of 2, when the bottom of the end-plates is lowered from the trailing edge by $0.1c$, C_l increased and C_d decreased as the ground is approached. Akimoto and Kubo [15] performed 2-D numerical simulations in ground effect using finite volume method. Shin [16] in his survey report compared the results from studies on NACA sections. Shin et al. [17] performed numerical simulation of viscous flow on NACA (4.6% thickness and 0.358% camber) and DHMTU S-shaped wings with end-plates at $Re = 4 \times 10^5$ and $h/c = 0.05$–0.7 at an aspect ratio of 1.0 and compared their results with experimental data. Yang and Shin [18] performed incompressible turbulent flow analysis of 2-D NACA thin wing section (4.6% thickness and 0.358% camber) at $Re = 10^6$ and $\alpha = 3.5$ deg and NACA6409 section at $Re = 2.37 \times 10^5$ and $\alpha = 4$ deg in ground effect using finite difference method. Ahmed and Goonaratne [19] reported results of their measurements on a 17% thick airfoil (wing of aspect ratio 0.13, provided with end-plates) at $Re = 3.6 \times 10^5$ for $\alpha = 0$–4 deg, $h/c = 0.025$–0.8, and flap angles of 0–10 deg. Chun and Chang [20] performed numerical simulations around two-dimensional airfoils in ground effect for Clark-Y section at $\alpha = 5.92$ deg, $h/c = 0.0483$, and $Re = 1.3 \times 10^6$ with a moving ground and NACA4412 section at $\alpha = 5$ deg, $h/c = 0.05$–0.8, and $Re = 2 \times 10^6$ with fixed and moving grounds and compared their results with experimental data available in the literature. Kikuchi et al. [21] reported results from their measurements on a NACA4412 airfoil (wing of aspect ratio 1.81) at $Re = 8 \times 10^5$, $\alpha = 0$–12 deg, and $h/c = 0.025$–0.4 in ground effect by method of towing. Ahmed and Sharma [22] performed experiments at $Re = 2.4 \times 10^5$ for $\alpha = 0$–10 deg and $h/c = 0.05$–1.0 on a NACA0015 airfoil in ground effect, whereas Ahmed [23] reported results from experiments on a NACA4415 airfoil at $Re = 2.4 \times 10^5$ for $\alpha = 0$–10 deg and $h/c = 0.05$–1.0 with fixed ground plates. Moon et al. [24] conducted numerical investigation on a NACA4406 wing of aspect ratio 2, provided with airfoil shaped end-plates at $Re = 2 \times 10^6$, $h/c = 0.025$–0.2 and presented results of lift and drag calculations. Studies reported in [25–31] were performed on inverted airfoils mainly for racing car applications. Ranzenbach and Barlow [25–27] demonstrated the ground effect for a single element airfoil configuration. They performed experiments and did numerical studies on single element symmetrical (NACA0015) and cambered (NACA4412) inverted airfoils (wings of aspect ratios 1.33 and 1.2, respectively, fitted in 2-D inserts) at $Re = 1.5 \times 10^6$. They found that the downforce reaches a maximum at a ground clearance of approximately $0.08c$; beyond this the airfoil and ground boundary layers were found to merge, which was given as the explanation for reduced downforce very close to the ground. Zhang et al. [28] reported the influence of tip vortex characteristics on the aerodynamic performance of an inverted cambered airfoil [modified GA(W) wing of aspect ratio 5 provided with end-plates] at $Re = 0.430$–0.462×10^6 and $h/c = 0.067$–0.448. Zerihan and Zhang [29] reported C_p, C_l, and C_d values on the same airfoil provided with end-plates. A flattened bottom surface was used to reduce the suction effect there. They found considerably higher suction on the upper (suction) surface as the ground was approached. The increased suction caused flow separation near the trailing edge, with the region of separated flow increasing in size as the airfoil was brought very close to the ground. Dominy (cited in [29]) postulated that in close proximity to ground, the airfoil stalls due to the adverse pressure gradient. In another paper, Zhang and Zerihan [30] investigated the wake behind the same inverted airfoil at the same Reynolds number using laser anemometry. Thus, it is clear that detailed experimental studies are performed only on inverted airfoils mainly for racing car applications. The flow characteristics for an inverted airfoil in ground effect are totally different compared with a regular airfoil in ground effect. The reducing gap between the suction surface and the ground enhances suction, whereas no significant effect is expected for the pressure surface. Interestingly, almost all the studies on inverted airfoils have found increasing C_d with reducing h [25–27,29]. In the case of a regular airfoil in ground effect, a high pressure is developed on the lower surface due to ramming action and the flow diversion towards the upper surface may enhance suction. Research efforts directed at the regular airfoil configuration in context of WIG craft are limited to force/pressure measurements and a complete understanding of the aerodynamics of ground effect is still lacking. A few detailed numerical works have been reported [11–13,15,17,18,20]. Some of the numerical results are inaccurate at low h due to interaction between airfoil and ground plate boundary layers [31]. Detailed studies of surface pressures, mean and fluctuating velocities over the surface and in the wake region of airfoil along with lift and drag forces need to be carried out for different airfoil configurations to gain insight into the fluid mechanics and to help the designers choose the right profile for applications in different WIG vehicles. Hayashi and Endo (cited in [11]) found that at lower Re (3.2×10^5) and relatively higher α, the flow separation phenomenon for an airfoil with ground effect was stronger than that without ground effect. The present work was undertaken to gain an insight into the basic fluid dynamics and to generate lift and drag data for a NACA4412 airfoil at a chord Re of 3.0×10^5.

III. Experimental Method

A. Wind Tunnel

The experiments were carried out at a velocity of 30.8 m/s in a return circuit low turbulence wind tunnel at the Institute of Fluid Science. The air flow in the tunnel was generated by an axial flow fan driven by a 95 kW dc motor. With the help of a thyristor system, it is possible to smoothly vary the speed of the motor and realize a velocity range of 5–80 m/s in the open test section. The airflow was discharged through the square outlet of the duct, having a side width of 800 mm, to the test section through a contraction nozzle with an area ratio of 12.

The mean velocity at the test section, having a length of 1420 mm, can be controlled with an accuracy of 1%. The freestream turbulence level at the velocity of 30.8 m/s was found to be about 0.07%. The variation in the mean velocity in the core region of the test section was found to be within 1% although the test section was open. Similarly, the flow velocity close to the moving belt surface was found to vary very little in the axial and transverse directions. The boundary layer thickness at the exit of the contraction nozzle was found to be about 30 mm. The boundary layer thickness was minimized by applying suction at the exit of the contraction nozzle. With the application of suction, the boundary layer became less than 1 mm thick at that station. Further details of the wind tunnel and the flow characteristics in the tunnel can be found in [32].

B. Moving Belt System

The moving belt used in the present studies has an effective length of about 1000 mm and a width of about 800 mm. Figure 1 shows a schematic diagram of the wind tunnel contraction outlet and of the moving belt system. The speed of the belt can be varied smoothly from 1 to 60 m/s with an increment of 0.1 m/s. The boundary layer thickness on the moving belt was found to be less than 1 mm at the beginning and slightly more than 2 mm at stations 700 mm downstream. This system is, hence, also suitable for testing tandem wing configurations [33].

C. Test Model and Experimental Setup

The airfoil chosen for the present work was NACA4412. This airfoil has been studied for its aerodynamic performance in ground proximity and it was thought that a good comparison can be made with the results available in the literature [11,20,21]. The chord length of the airfoil is 150 mm and the span is 600 mm. Forty pressure taps were provided (including one each at the leading and the trailing edges) on the surface of the airfoil in an X-configuration for measurement of pressure distribution. End-plates were provided on the sides of the wing model to improve its aerodynamic performance [9,14] by achieving a two-dimensional flow over the model (airfoil characteristics). Many WIG vehicles employ end-plates to take advantage of the improved aerodynamic performance. The spacing between the plates was 600 mm (wing span), as shown in Fig. 2. The assembly of the wings and the end-plates (henceforth, it will be called the test model) was positioned over the moving belt system in the open test section and was held with the help of four steel wires having a diameter of 0.75 mm.

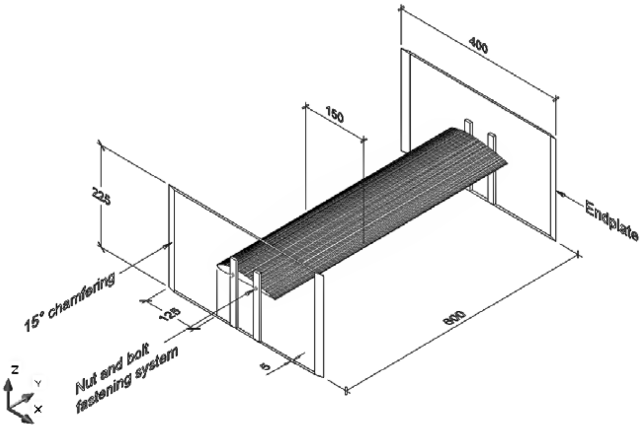

Fig. 2 Schematic diagram of the test model.

The length of the end-plates is a very important factor which strongly influences the flow characteristics over the airfoil. It was decided to provide an optimum length of the end-plates ahead (upstream) of the airfoil to keep the boundary layer thickness on the plates to a minimum without allowing the streamlines to divert away from the test model. A long length ahead of the leading edge may result in a thick boundary layer on the inner side of the end-plates causing a spanwise component towards the midspan, whereas a smaller length may cause flow diversion away from the test model due to blockage, resulting in a spanwise component away from the midspan. After some preliminary work, it was decided to have end-plates with a length of 400 mm, with 125 mm ahead of the leading

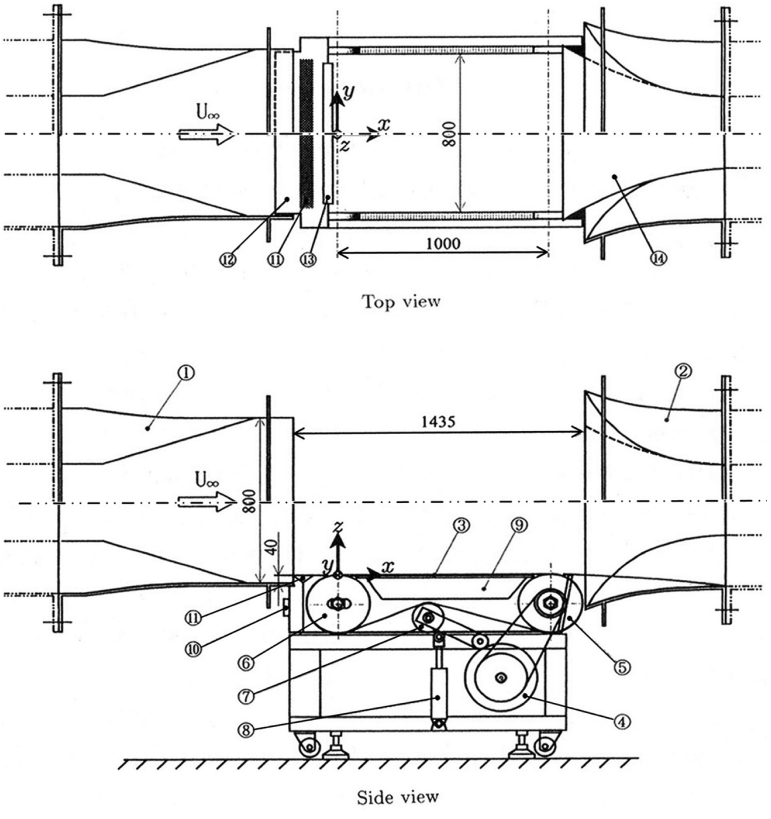

Fig. 1 Schematic diagram of the test section and moving belt system.

edge of the airfoil to ensure a 2-D flow. The end-plates had a height of 225 mm ($1.5c$) to prevent flow leakage into or out of the test model due to any pressure difference between inside and outside the test model (earlier studies [22] had shown that the presence of the airfoil affects the velocity field almost up to half the chord length distance over the airfoil surface in the vertical direction).

The experiments involved measurements of the surface pressure distribution, lift and drag forces, mean velocity, and turbulence intensity over the airfoil surface and in the wake region. Initial measurements were performed with a TSI Nd:YAG laser-based particle image velocimetry (PIV) system to examine the nature of the flow. The 532 nm output of the laser was converted to a laser sheet and delivered at the desired location by a LASERPULSE Light Arm. The system was controlled through a Synchronizer, model 610032, and the camera used was PIVCAM, model 630046. The pressure measurements in the present work were performed with the help of a pneumatic intelligent pressure scanner, model 9016. The scanner integrates 16 pressure sensors having a range of 2.5–5200 kPa (absolute) with a microprocessor; the data from the sensors were fed to a PC. A six-component Gottingen-type wind tunnel balance was used to measure lift [32]. For measurement of drag, a dynamic strain amplifier was used. Both the balance and the amplifier were calibrated for force measurements. A single-component hot-wire anemometry system, consisting of a constant temperature anemometer (CTA) unit and a signal conditioner were used in the present investigation. The tungsten wire, used in the present investigation, has a diameter of 5 μm. The data from the anemometer were fed to a PC. At each measurement location, about 12,000 samples were acquired to calculate the mean and rms velocities. A computer-controlled microprocessor-based stepper-motor-driven traverse system was used for traversing the hot-wire probe to various locations in the test section.

D. Experimental Procedure

The mean velocity in the test section was set to 30.8 m/s with the help of the thyristor system. The velocity was also measured with the help of the calibrated hot-wire anemometer to ascertain that the variations are within 1% of this value. The belt speed was kept equal to U_∞ for all experiments. The test variables were incremented gradually to study each effect separately. However, only a few results are presented in this paper. The Reynolds number, based on the freestream velocity of 30.8 m/s and the chord length, was 3.0×10^5. An impact tube was used for measuring the total pressure. The hot-wire anemometer was calibrated against the impact tube. The model was held in the test section at the desired α. The end-plates had a length of 400 mm, with 125 mm ahead of the leading edge of the airfoil, as explained earlier. Two-dimensional nature of the flow was ensured before proceeding with the actual measurements by performing PIV measurements. Figure 3 shows the results of PIV measurements over the airfoil surface for $\alpha = 0$ deg and $h/c = 1.0$.

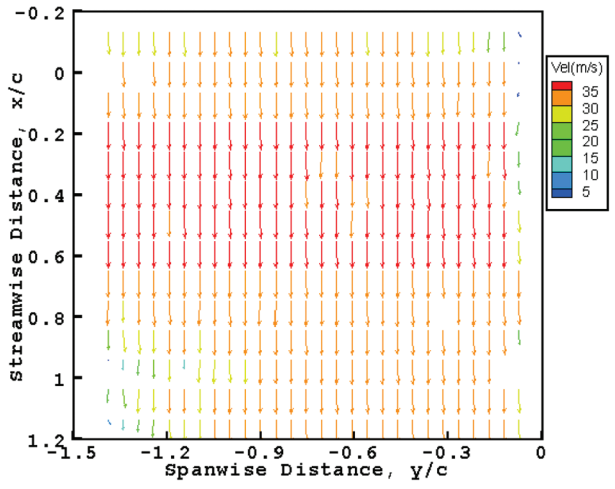

Fig. 3 Velocity vectors over the airfoil for $\alpha = 0$ deg and $h/c = 1.0$.

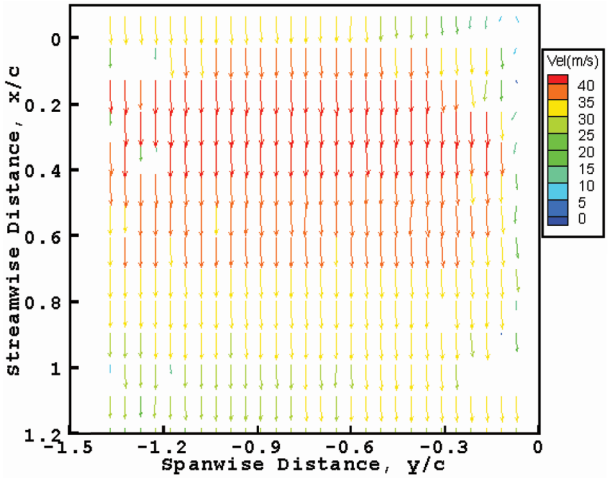

Fig. 4 Velocity vectors over the airfoil for $\alpha = 10$ deg and $h/c = 1.0$.

Measurements were performed at $0.1c$ above the airfoil. To calculate the velocity, averaging was done over 50–100 measurements. One set of photographs was obtained in 50 μs. The two-dimensional nature of the flow (vectors in streamwise direction) and the acceleration over the surface can be noted from the figure. As the interference is small for this angle, a fully 2-D flow was expected. For the higher α of 10 deg, the flow characteristics were studied in detail to ensure 2-D flow. Figure 4 shows the velocity vectors for $\alpha = 10$ deg and $h/c = 1.0$. A high blockage to the flow is expected for this case, which may cause flow diversion away from the test model. However, the velocity vectors indicate a clearly streamwise flow. The acceleration of flow over the surface is higher for this ground clearance compared to $h/c = 0.05$ (not shown) which is supported by pressure measurements and velocity measurements. As the air moves towards the trailing edge, the streamwise component of velocity reduces due to downwash. A comparison of Figs. 3 and 4 clearly shows the effect of α ($x = 0$ corresponds to the leading edge). The higher acceleration near the leading edge and the deceleration towards the trailing edge due to the adverse pressure gradient for $\alpha = 10$ deg can be seen. It can also be seen that the highest velocity (indicating suction peak) is very close to the leading edge for $\alpha = 10$ deg and away from the leading edge for $\alpha = 0$ deg. For $\alpha = 10$ deg and $h/c = 0.05$, measurements were performed perpendicular to the flow direction to get an idea of the flow components in the y- and z-directions. Figure 5 shows the velocity vectors for this case (looking at the airfoil from the trailing-edge side). Thus, the vectors in the z-direction indicate the downwash (flow vertically downwards with negative velocities) and the vectors in the y-direction show the magnitude of the spanwise component. It

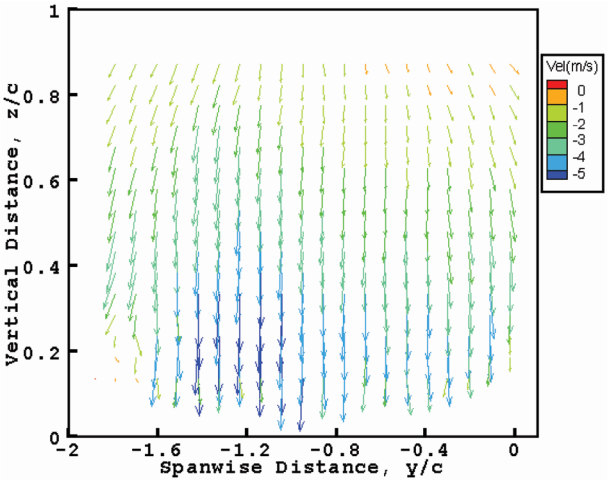

Fig. 5 Velocity vectors normal to the flow direction for $\alpha = 10$ deg and $h/c = 0.05$.

Table 1 Location on the upper surface (x/c) where boundary layer transition was detected

α	$h/c = 0.05$	$h/c = 1.0$
0 deg	0.77	0.73
4 deg	0.58	0.55
10 deg	0.17	0.14

can be seen that the spanwise component is negligibly small with a maximum velocity of about 2 m/s.

Experiments were performed by varying α from 0 to 10 deg. The vertical position of the airfoil with respect to the end-plates was varied to get h/c values of 0.05–1.0. Readings from the wind tunnel balance and the dynamic strain amplifier were recorded. Over the airfoil surface and in the wake region, hot-wire probe was traversed from 2 mm above the surface to about 150 mm. Over the airfoil, traverses were made at four axial locations of $x/c = 0.05, 0.35, 0.7$, and 0.9, whereas in the wake region, measurements were performed at two axial locations of 75 mm ($0.5c$) and 150 mm ($1.0c$) from the trailing edge of the airfoil. In these sets of experiments, measurements were not performed very close to the surface (z or $z' = 1$ mm) to avoid frequent breakage of the hot-wire especially in the wake region where the belt was moving underneath. However, to get information on the airfoil boundary layer, measurements were performed very close to the airfoil surface for a few cases. The boundary layer on the airfoil was found to be laminar on the upper surface near the leading edge but became turbulent later on. In the Re range of 1.0×10^5–6.0×10^5, transition to turbulence is known to take place through a laminar separation bubble. The separated flow forms a free shear layer which is highly unstable and soon transits to turbulent. While undergoing transition, the separated shear layer gains enough energy to overcome the adverse pressure gradient and reattaches to the surface of the airfoil, completing the separation bubble. The size of the separation bubble becomes smaller with increasing Reynolds number [34]. No attempt was made to perform a detailed study of the separation bubble and its characteristics, as that was not the aim of this work. Measurements were performed only to get information on the location of transition. The displacement thickness and the turbulence intensity are maximum at the location of transition. However, the presence of reverse flow alters the numerical value of displacement thickness [35], whereas it is easier to measure the maximum turbulence intensity. The streamwise location of transition is, therefore, commonly identified with the peak turbulence intensity. Table 1 lists the location on the upper surface where transition was detected (location of maximum turbulence intensity) at the smallest and largest ground clearance. It is interesting to note that the location of transition moves downstream on the airfoil surface when the airfoil is brought close to the ground.

The accuracy of measurements of C_p was estimated by calculating dC_p from the expression for C_p (i.e., $C_p = [p - p_\infty]/0.5\rho U_\infty^2$). Thus, the measurements of C_p in the present studies were made with an accuracy of 1.4%. The accuracy of measurements of velocity was estimated following the procedure in [36]. The accuracies of calibration and conversion (uncertainty related to curve-fitting errors) were taken into consideration for estimation of error. As the calibration was performed with the help of impact tube, the maximum error in the measurement of velocity was estimated to be about 2.2%. The conversion accuracy was estimated to be within 1.5%. A large number of samples was acquired to reduce the uncertainty level of turbulence intensity measurements, following the procedure in [36]. The uncertainty in the measurement of turbulence intensity was within 2.6%. The repeatability of force measurements was within $\pm 0.9\%$, whereas that of pressure and velocity measurements was within $\pm 1.3\%$.

IV. Results and Discussion

The results are presented and discussed in this section. For calculation of C_p, the measured static pressure at a location is nondimensionalized with respect to the freestream static pressure and the freestream mean velocity (U_∞). All mean and fluctuating velocities are nondimensionalized with respect to U_∞.

A. Surface Pressure Distributions

Figures 6–9 show the variation of C_p on the surface of the airfoil with ground clearance, for angles of attack of 0, 4, 8, and 10 deg, respectively, (for all these figures, the distributions on the lower side show the lower surface pressures and those on the upper surface show the upper surface pressures, except for $\alpha = 0$ deg and $h/c = 0.05$). Figure 6 shows the variation in the pressure on the airfoil surface for $\alpha = 0$ deg at different values of h/c. The pressure is high on the lower surface at points very close to the leading edge. A very interesting observation in this case is a suction effect on the lower surface at small ground clearances, although the pressure is positive and high at the first measurement point. This is because the area between the airfoil and the ground forms a convergent-divergent passage, and its effect is more prominent for lower ground clearances. The NACA4412 airfoil at $\alpha = 0$ deg has its lowermost

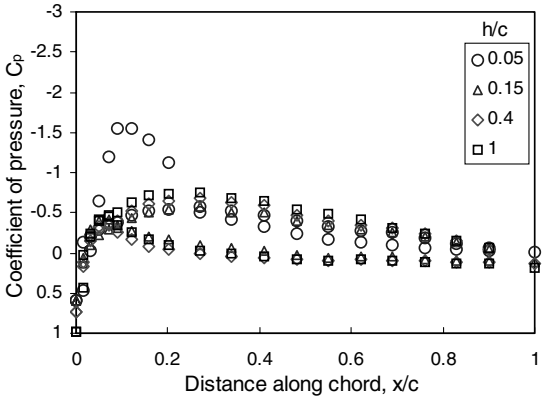

Fig. 6 Pressure distribution on the surface of the airfoil at $\alpha = 0$ deg.

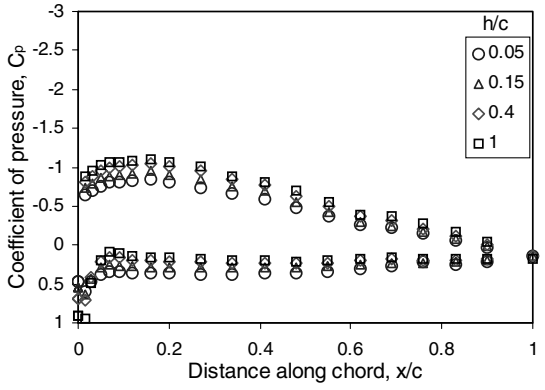

Fig. 7 Pressure distribution on the surface of the airfoil at $\alpha = 4$ deg.

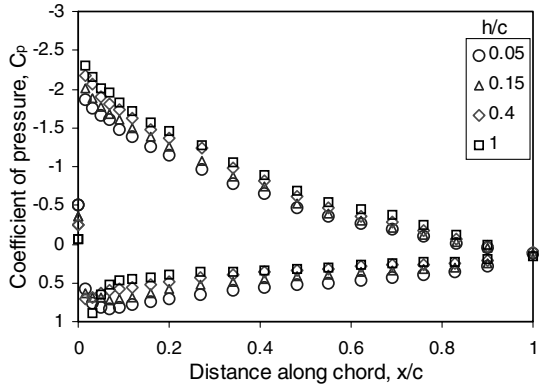

Fig. 8 Pressure distribution on the surface of the airfoil at $\alpha = 8$ deg.

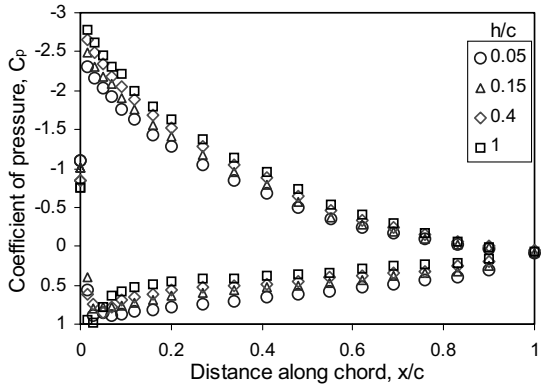

Fig. 9 Pressure distribution on the surface of the airfoil at $\alpha = 10$ deg.

point at 11% of the chord length. This is the location where minimum pressure is expected and recorded with a C_p value of -1.56. Downstream of this point, there is a divergent flow path under the airfoil giving rise to an adverse pressure gradient. The pressure gradient is very high for $h/c = 0.05$, which resulted in flow separation from the surface. The distribution of canonical pressures was plotted for this case. A knowledge of canonical pressures is known to be extremely useful for separation analysis [25,37]. Canonical pressures allow pressure recoveries to be compared directly as long as the Reynolds number based on the momentum thickness at the start of the pressure recoveries are similar [25,37]. It is found that the flow separates from the surface at $x/c = 0.598$. An abrupt increase in pressure following the constant pressure region serves as an indication of the position of the reattachment point [38]. Thus, it is clear that the flow fails to reattach. Although laminar separation (without reattachment) is not common at this Reynolds number, the decelerated flow under the lower surface, due to the constricted passage, fails to overcome the rising pressure and leaves the surface. The result of this separation is a significant loss of lift, and will be discussed later. Kikuchi et al. [21] also reported a strong suction on the lower surface for $\alpha = 0$ deg and $h/c = 0.1$ which resulted in a loss of lift (discussed in Sec. IV.D).

Another interesting observation from the C_p plots is a reducing suction on the upper surface with reducing h. An increased suction was expected on the upper surface due to flow diversion towards the upper surface; however, the maximum suction was recorded for the highest ground clearance of $h/c = 1.0$. For $h/c = 0.05$, a higher suction was observed in a small region from $x/c = 0.03$–0.2 compared to $h/c = 0.15$; the lowest point on the lower surface is almost touching the ground for this case, hence the flow is diverted over the airfoil. For $h/c = 1.0$, the streamline convergence on both sides of the airfoil causes an increase in velocity on both the sides as there will be a reduction in pressure compared with the freestream pressure, thus resulting in negative C_p values. Further downstream, the C_p values become positive on the lower surface as the pressure increases due to an increase in the flow area.

The suction effect on the lower surface disappears when α is increased to 2 deg (not shown). When α is further increased to 4 deg, the passage under the airfoil becomes convergent; hence, pressures at all the points on the lower surface are found to be positive and the pressure gradients are favorable for all values of h/c. Although the pressure is higher on the lower surface at small ground clearances, the lift force is lesser due to the loss of suction on the upper surface. Thus, the lift force reduces as the ground is approached for $\alpha = 4$ deg (Sec. IV.D). Similar results were obtained by Hsiun and Chen [11] for the same airfoil who reported a reduced lift force at $h/c = 0.05$ due to a loss of suction on the upper surface for $\alpha = 5$ deg. Chun and Chang [20] also reported a loss of suction on the upper surface for NACA4412 as the ground was approached for both the cases of fixed and moving grounds for $\alpha = 5$ deg. Kikuchi et al. [21], on the other hand, did not find any appreciable change in the upper surface suction for the same airfoil for $\alpha = 4$ and 6 deg when the ground was approached. Yang and Shin [18] reported a loss of upper surface suction for NACA6409 as the (moving) ground was approached for $\alpha = 4$ deg.

It is interesting to note that although the net suction on the entire upper surface is reducing with h, the suction peak is likely to be higher at the smallest h/c. This is supported by the fact that the suction at the leading edge increases with reducing h/c and is highest at the smallest h/c and also by the previous works on this airfoil [11,20,21].

Figure 8 shows the pressure distributions on the surface of the airfoil for $\alpha = 8$ deg and different ground clearances. For this α, the pressure rise on the lower surface with reducing ground clearance is appreciable. As a result, the lift is found to increase as the airfoil approaches the ground although there is a loss of upper surface suction in close ground proximity. For the same α, Kikuchi et al. [21] also reported increased lift in close ground proximity mainly due to higher pressures on the lower surface.

At $\alpha = 10$ deg, the values of C_p are very high on the pressure side for the smallest ground clearance of $h/c = 0.05$. With increasing h/c, the pressure drops, as depicted in Fig. 9. It is interesting to compare the pressure distribution on the lower surface in Figs. 7 and 9. The increased pressure and the shifting of the stagnation point downstream for higher α can clearly be seen, although the stagnation pressure was not recorded for all the cases due to the relatively coarse measurement grid. The upper surface suction is found to be the strongest for $\alpha = 10$ deg, resulting in a strong adverse pressure gradient due to the high flow divergence angle in the downstream direction. However, the flow remained attached to the surface for all ground clearances. As discussed earlier, there is a loss in upper surface suction with reducing h. Hsiun and Chen [11] also reported loss of upper surface suction at $Re = 2 \times 10^5$ at the same α for the same airfoil. It was reported earlier that at lower Re (3.2×10^5) and relatively higher values of α, the flow separation phenomenon of the airfoil with ground effect was stronger than that without ground effect [11]. However, the results for NACA4412 indicate that this statement is not valid for all airfoil geometries, but for those geometries for which the suction gets enhanced with reducing h. Ahmed [23] reported flow separation at $Re = 2.4 \times 10^5$ at $\alpha = 10$ deg for $h/c = 0.05$ and $h/c = 0.1$ for NACA4415. In his case, enhanced upper surface suction was recorded with reducing h resulting in a strong adverse pressure gradient. The transition of the upper surface boundary layer to turbulent through a separation bubble deteriorates the performance of the airfoil. It is a bad starting condition of a turbulent boundary layer. The boundary layer will be thicker and hence will be more sensitive to adverse pressure gradients and likely to separate from the surface. While the skin friction is low in the bubble, the pressure drag is increased and may cause a thicker wake.

B. Velocity Survey over the Airfoil

Distributions of mean velocity (u/U_∞) and turbulence intensity ($\sqrt{\overline{u'^2}}/U_\infty$) over the surface of the airfoil were obtained by making detailed measurements of velocity from (z=) 2 mm above the airfoil to 150 mm and $x/c = 0.05$–0.9 at different ground clearances at the midspan section. As reported earlier, measurements were not performed at $z = 1$ mm to avoid frequent breakage of the hot-wire; hence the mean velocity distributions presented in this section do not provide information on the maximum velocity over the airfoil surface.

Figure 10 shows the variation of mean velocity (right-side profiles) and turbulence intensity (left-side profiles) along the chord length of the airfoil for $\alpha = 4$ deg and $h/c = 0.4$. A logarithmic scale was chosen for the mean velocity and turbulence intensity. A stronger suction effect near the leading edge on the upper surface gives rise to accelerated flow there. As the flow moves towards the trailing edge, it has to overcome an adverse pressure gradient; hence the velocity close to the surface reduces to overcome this gradient. However, it can be seen from the profile that, due to gradual pressure recovery, the flow remains attached to the upper surface of the airfoil and the turbulence levels remain low.

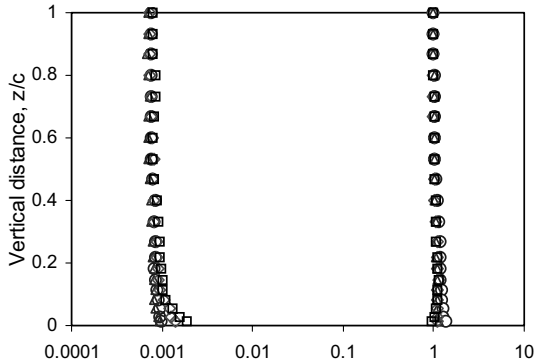

Fig. 10 Distributions of mean velocity (right) and turbulence intensity (left) over the surface of the airfoil at $\alpha = 4$ deg and $h/c = 0.4$; ○—$x/c = 0.05$, △—$x/c = 0.35$, ◇—$x/c = 0.7$, □—$x/c = 0.9$.

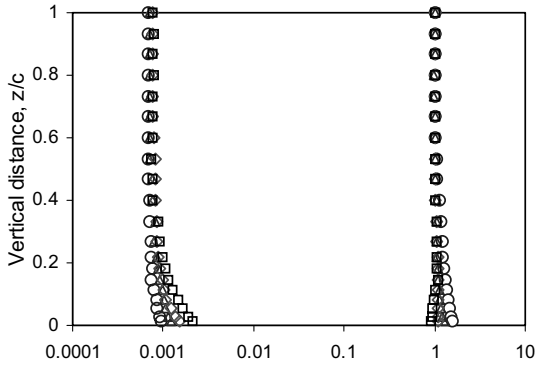

Fig. 11 Distributions of mean velocity (right) and turbulence intensity (left) over the surface of the airfoil at $\alpha = 10$ deg and $h/c = 0.05$; ○—$x/c = 0.05$, △—$x/c = 0.35$, ◇—$x/c = 0.7$, □—$x/c = 0.9$.

Figure 11 shows the variation of velocity over the surface for $\alpha = 10$ deg and $h/c = 0.05$. A higher mean velocity over the airfoil surface at $x/c = 0.05$ compared to Fig. 10 shows a higher suction. The flow loses its kinetic energy rapidly in overcoming the adverse pressure gradient, shown in Fig. 9, as it moves towards the trailing edge. The distributions of mean velocity and turbulence intensity for $\alpha = 10$ deg and $h/c = 0.4$ are shown in Fig. 12. As discussed earlier (Fig. 9), the upper surface suction is very high for this case, resulting in a considerably higher velocity (about 80% greater than the freestream velocity) 2 mm above the surface. The velocity reduces towards the trailing edge and the turbulence level rises. The higher turbulence level may be due to a thicker boundary layer that is expected due to the adverse pressure gradient. It is interesting to see that the mean velocity at the last station ($x/c = 0.9$) for this case is less than that for $h/c = 0.05$, although it was higher near the leading edge, showing a higher deceleration (higher pressure recovery, shown in Fig. 9). For both the cases, the mean velocity at $x/c = 0.9$ is less than the freestream velocity.

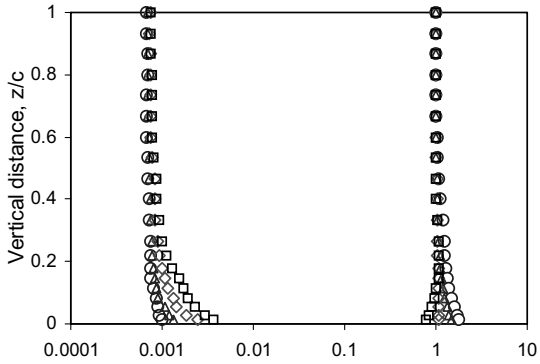

Fig. 12 Distributions of mean velocity (right) and turbulence intensity (left) over the surface of the airfoil at $\alpha = 10$ deg and $h/c = 0.4$; ○—$x/c = 0.05$, △—$x/c = 0.35$, ◇—$x/c = 0.7$, □—$x/c = 0.9$.

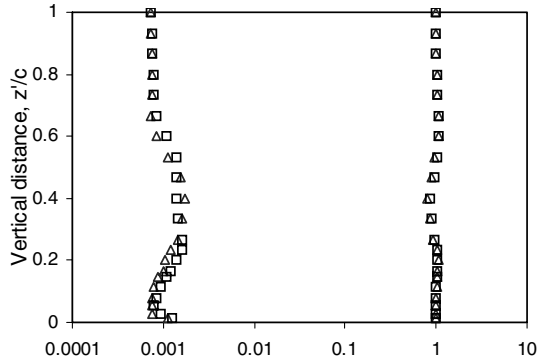

Fig. 13 Distributions of mean velocity (right) and turbulence intensity (left) in the wake region of the airfoil for $\alpha = 4$ deg and $h/c = 0.4$; △—$l/c = 0.5$, □—$l/c = 1.0$.

C. Wake Studies

In the wake region, measurements of mean velocity and turbulence intensity were performed at two axial locations: 75 and 150 mm from the trailing edge (which correspond to $0.5c$ and $1.0c$, respectively), from 2 mm above the ground to 150 mm at different ground clearances. Figure 13 shows the distributions of mean velocity and turbulence intensity in the wake region for $\alpha = 4$ deg and $h/c = 0.4$. It can be noted that the maximum defect in velocity profile and the peak in turbulence intensity correspond to approximately the height equal to the ground clearance of the airfoil for lower values of α. The mean velocity and turbulence intensity values were integrated from $z'/c = 0.02$–1.0 to obtain the drag force. At higher values of α, the viscous stress (the contribution of Reynolds stress) was also accounted for, as the wake turbulence has a significant effect on the drag coefficient [39]. The values of drag coefficient were in good agreement with the measured values reported in the next section.

For small values of α, the defect in mean velocity profile was found to be small and the turbulence levels were low, indicating a small momentum loss. A larger defect in mean velocity profiles and higher turbulence levels are observed for $\alpha = 10$, as can be seen from Figs. 14 and 15. For $h/c = 0.05$, the velocity defect is larger at $l/c = 0.5$ and slightly away from the ground (Fig. 14). At the subsequent station, the low velocity region moves very close to the ground due to spreading of the shear layer. It can be seen from the plots of mean velocity and turbulence intensity that the profiles tend to become uniform as l/c increases. The momentum loss is considerably higher for $\alpha = 10$ deg and $h/c = 0.4$ compared to $\alpha = 4$ deg, as can be seen from a comparison of Figs. 13 and 15, indicating a higher drag. The turbulence level is also higher for the

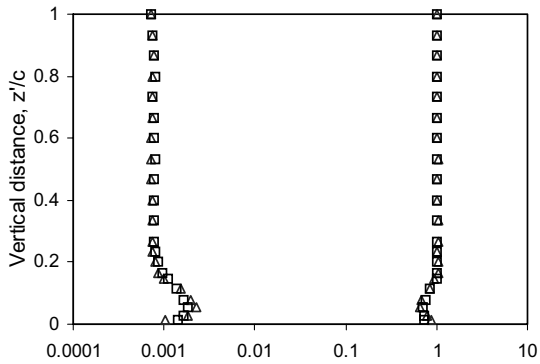

Fig. 14 Distributions of mean velocity (right) and turbulence intensity (left) in the wake region of the airfoil for $\alpha = 10$ deg and $h/c = 0.05$; △—$l/c = 0.5$, □—$l/c = 1.0$.

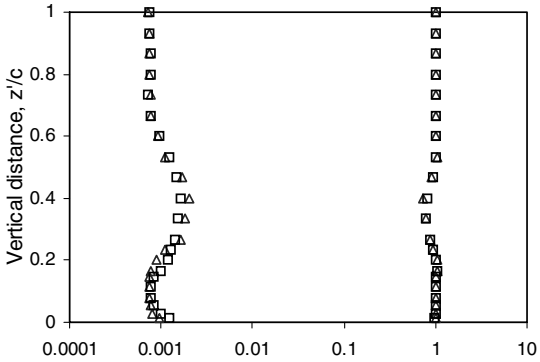

Fig. 15 Distributions of mean velocity (right) and turbulence intensity (left) in the wake region of the airfoil for $\alpha = 10$ deg and $h/c = 0.4$; △—$l/c = 0.5$, □—$l/c = 1.0$.

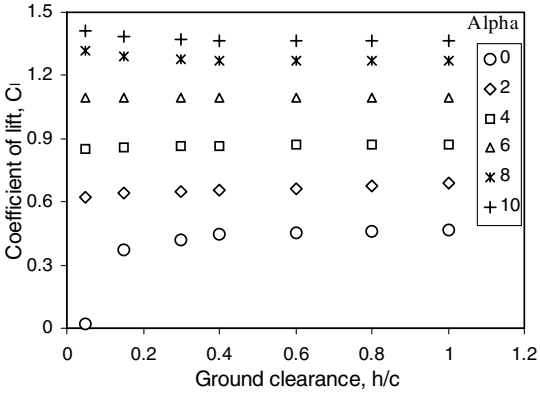

Fig. 16 Coefficient of lift at varying ground clearances for different angles of attack.

higher α. However, the contribution of the turbulence term was found to be small compared to the momentum loss for all cases.

D. Lift and Drag Coefficients

Figures 16 and 17 present the results of lift and drag measurements for different values of α and h/c. The lift force was found to reduce with h for angles up to 4 deg, remain constant with changing h for 6 deg, and increase with reducing h for higher angles of 8 and 10 deg. For $\alpha = 0$ deg, the lift force is almost zero at $h/c = 0.05$ due to the strong suction effect on the lower surface and the laminar separation, shown in Fig. 6. However, integration of the pressure distribution gave a small negative lift coefficient for this case. Kikuchi et al. [21] reported a relatively weaker suction effect on the lower surface for the same airfoil at $\alpha = 0$ deg and $h/c = 0.1$ and a low value of C_l (they did not make measurements at $h/c = 0.05$). Tomaru and Kohama [10] recorded negative values of C_l for NACA23012 for

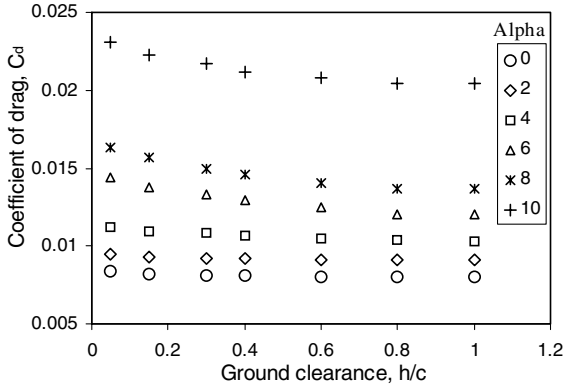

Fig. 17 Coefficient of drag at varying ground clearances for different angles of attack.

$h/c < 0.15$. The NACA23012 section has a convergent-divergent passage under the airfoil for 0 deg, with a pretty long flattish region between $x/c = 0.27$ and 0.43. A strong suction effect is thus expected for this airfoil at 0 deg, which increases with reducing h, causing C_l to drop; the C_l value thus continuously dropped with reducing h. There may be laminar separation at the smallest h, which resulted in negative C_l. Similar results were reported by them for NACA0012-64 with negative values of C_l for low h for $\alpha = 0$ deg. For NACA6412 airfoil, they recorded a lower C_l for $\alpha = 0$ deg at $h/c = 0.05$. For this h, the lower surface of NACA6412 will almost touch the ground; hence, it is expected that the flow velocity will be very small under the airfoil. The passage under the airfoil is then divergent with a good divergence angle between $x/c = 0.1$ and 0.3. The strong suction and possible laminar separation are the apparent causes of the reduced lift. For a 15% thick symmetrical Joukowski airfoil at $\alpha = 0$ deg, Coulliette and Plotkin [12] reported continuously reducing C_l values with reducing h (they defined h as the height of the midchord point) due to lower surface suction. The suction effect on the lower surface can be reduced if the airfoil has a flatter bottom. Fink and Lastinger [6] experimented a modified airfoil with a flat bottom from $0.3c$ to $1.0c$ and found that C_l remains approximately the same with changing h for $\alpha = 0$ deg. They suggested that airfoils with a high camber (apart from a flat bottom) should be employed in ground effect machines that operate near 0 deg angle of attack to obtain a reasonably high C_l.

For $\alpha = 2$ and 4 deg, the lift force reduced continuously but slowly with reducing h. For both these angles, the pressure on the lower surface increased with reducing h, as discussed earlier; however, there is a loss of upper surface suction as the airfoil approaches the ground. From Fig. 7, it is clear that this loss is greater compared with the gain on the pressure side; as a result, the lift drops with h. For 3 deg, Coulliette and Plotkin [12] observed that C_l increased slightly and then decreased sharply with reducing h due to suction effect. For NACA0012-64, Tomaru and Kohama [10] found a reduction in C_l close to the ground for $\alpha = 2.5$ deg. Chun and Chang [20] also reported a loss of suction on the upper surface for NACA4412 as the ground was approached for both the cases of fixed and moving grounds for $\alpha = 5$ deg. For $\alpha = 5$ deg, Coulliette and Plotkin [12] reported an increase in C_l when h/c was reduced up to 0.2 for the 15% thick symmetrical airfoil; close to the ground, C_l decreased. Hsiun and Chen [11] reported a reduced lift force for NACA4412 at $h/c = 0.05$ due to a loss of suction on the upper surface for $\alpha = 5$ deg; however, the boundary condition of $u = 0$ applied by them at the ground plane (fixed ground) was questioned by Steinbach [40], who also opined that at this α, C_l can not suddenly reduce when h/c is reduced to 0.05. In fact, the C_l at small ground clearances for this α is found to be higher with fixed ground compared to moving ground by Chun and Chang [20]. For a fixed ground, the increasing thickness of the boundary layer towards the trailing edge causes an additional pressure rise on the lower surface due to conversion of the kinetic energy to pressure energy. The boundary layer may plug up the trailing edge gap and prevent the flow from exiting; in the limiting case of zero trailing-edge gap, the flow will stagnate with a fixed ground whereas with a moving ground there will be a large trapped vortex below the airfoil which is driven be viscous effects from the moving ground. Moreover, for given values of α and h/c, the boundary layer on the fixed ground causes an escape flux over the airfoil resulting in a higher suction on the upper surface compared to the moving ground which further increases the lift [20]. The combined gain will be higher than the loss resulting from a reduced ramming effect close to the leading edge compared to the moving ground case. At small ground clearances, the moving ground acts as a pump accelerating the flow through the gap. Ahmed and Goonaratne [19] reported a slight increase in C_l when h/c was reduced from 0.075 to 0.03 for $\alpha = 2$ deg. Yang and Shin [18] found increasing C_l as the ground was approached for NACA6409 at $\alpha = 4$ deg although there was a loss of upper surface suction. The results for 6 deg in the present work are very interesting with constant values of C_l for all ground clearances investigated, indicating that the gain on the pressure side with reducing h is just balanced by the loss of suction on the suction side (the pressure measurements were not performed for

this case). Most of the other investigators (Fink and Lastinger [6], Fuwa et al. [8], Tomaru and Kohama [10], Chun et al. [14]) reported increasing lift with reducing h for this α.

When α is increased to 8 deg, a considerable increase in pressure on the lower surface was observed which resulted in a higher lift force in close ground proximity although there is a loss in upper surface suction. As discussed earlier, the stagnation point moved downstream on the lower surface when h is reduced. The downward shift of the stagnation point also increases the lift directly, as the lower surface stagnation point will have a significant lift component. A leading-edge stagnation point does not have a force component in the direction of lift. For $\alpha = 10$ deg, the lift force was found to be constant when h/c was reduced from 1.0 to 0.4 and then increase as the ground was approached. This is due to the increased pressure on the lower surface, although there is a loss in upper surface suction for this α also. Kikuchi et al. [21] reported similar results for the same airfoil at the same angles of 8 and 10 deg, although the increase in C_l close to the ground was higher in their case. On the other hand, Hsiun and Chen [11] reported a reduced value of C_l for the same airfoil at $h/c = 0.05$ for $\alpha = 10$ deg at $Re = 2 \times 10^5$ due to a higher loss of upper surface suction compared to the gain in the lower surface pressures. Zerihan and Zhang [29] in their paper concluded that the lift force (downforce in their case, as the airfoil was inverted) increases with reducing h, whereas very close to the ground, the lift force reduces due to flow separation from the upper surface. For an inverted airfoil, the suction on the suction surface is always enhanced close to the ground. Although enhanced suction is always desirable to get higher lift, it also means greater deceleration towards the rear. For any type of trailing edge, the flow decelerates to below freestream values. If the deceleration is too severe, separation occurs.

The results of drag measurements for different values of α and h are shown in Fig. 17. The measured drag force was decomposed into its pressure drag and skin friction drag components for some of the cases by finding the pressure drag from integration of the pressure distributions reported in Figs. 6–9. The drag force increases a little with reducing h for $\alpha = 0$–4 deg, whereas a higher increase is observed for 6–10 deg. For $\alpha = 0$ deg and $h/c = 0.05$, the lower surface suction and separation cause an increase in the pressure drag, as NACA4412 airfoil has a slightly divergent path under it at this angle after the minimum pressure point. The region of high suction on the lower surface ($x/c = 0.1$–0.2) is almost horizontal, hence it does not contribute much to the pressure drag; however, the extended region of low pressure further increased the pressure drag. The contribution of pressure drag to the total drag for $\alpha = 0$ deg is slightly less than 40% for $h/c = 0.15$–1.0, but increased for $h/c = 0.05$. The shifting of the transition point downstream with reducing h reduces the region of turbulent flow and the skin friction drag for all angles of attack, whereas the loss of upper surface suction (lower velocity) with reducing h increases the skin friction drag. Also, the lower velocity under the lower surface increases the skin friction drag. For $\alpha = 0$ and 2 deg, the higher upper surface suction at higher h has a larger component in the direction opposite to drag compared to that in the direction of drag, resulting in a lower pressure drag when the airfoil is away from the ground. For $\alpha = 2$ deg, although the lower surface pressure increases at low h [21], it does not increase the pressure drag because the airfoil has a nearly horizontal lower surface from $x/c = 0.1$ to 1.0 at this angle. A combination of these factors results in a slightly higher drag close to the ground for these two angles. Similar trends for C_d are reported by Kikuchi et al. [21] for the same airfoil. For NACA23012, and NACA0012-64, Tomaru and Kohama [10] reported similar results for $\alpha = 0$ and 2.5 deg. Ahmed and Goonaratne [16] found a very small decrease in C_d values as h/c was reduced from 0.075 to 0.03 for $\alpha = 2$ deg.

Another factor which affects the pressure drag to some extent is the downward shift of the stagnation point with reducing h. A leading-edge stagnation point has a significant contribution to the pressure drag. On the other hand, if the stagnation point shifts towards the lower surface, there will be a reduced component of the high force in the drag direction; moreover, this will cause suction at the leading edge, which will directly reduce the pressure drag.

For $\alpha = 4$ and 6 deg, a higher pressure on the lower surface with reducing h (Fig. 7) increases the pressure drag; at the same time, the contribution of upper surface suction in the direction opposite to drag with increasing h is slightly lesser for these angles compared to 0 and 2 deg. However, interestingly, for $\alpha = 4$ deg, the contribution of pressure drag to the total drag remained at about 40% for all ground clearances. The drag increase with reducing h is higher for 6 deg compared to 4 deg, a trend also reported by Kikuchi et al. [21] for NACA4412. Hsiun and Chen [11] reported reducing C_d with a reduction in h/c for 5 deg, a trend also reported by Chun and Chang [20] for the fixed ground case. With the moving ground, Chun and Chang [20] reported nearly constant values of C_d with changing h for the same airfoil. It is interesting to note from their results that at low h, the drag is lower with the fixed ground, whereas for high h values, C_d is higher with the fixed ground. The escape flux towards the upper surface with the fixed ground reduces the pressure drag at lower angles of attack because there will be a larger component of the force in the negative drag direction, the magnitude of which depends on the airfoil geometry. At higher angles of attack, the pressure drag may be higher because the part of the airfoil after $x/c = 0.4$ is now at a higher inclination, resulting in a larger component in the positive drag direction. Shin et al. [17] reported a slight increase in C_d with reducing h for $\alpha = 3.5$ deg. Fink and Lastinger [6] reported slightly reducing values of C_d with reducing h for $\alpha = -5$–10 deg for different aspect ratios. Increasing C_d values with h were reported by Chun et al. [14] for NACA6409 at α ranging from 0 to 8 deg.

For $\alpha = 8$ and 10 deg, the drag increased appreciably with reducing h mainly due to the considerably higher contribution of the increased pressure on the lower surface to positive pressure drag. The drag at all ground clearances is higher for 10 deg compared with the lower angles mainly because of the higher pressure drag from both the surfaces; there is hardly any negative pressure drag for this α. The contribution of the pressure drag to the total drag, which was about 65% for $h/c = 1.0$, increased to about 68% for $h/c = 0.05$. The momentum loss and turbulence levels for this α are significantly higher compared with the lower angles (Figs. 13–15). The thicker wake region and higher turbulence levels may be due to flow separation before the trailing edge. Very similar results were obtained by Kikuchi et al. [21] for the same airfoil for this α. Hsiun and Chen [11] reported a lower value of C_d for NACA4412 airfoil at $h/c = 0.05$ for $\alpha = 10$ deg at $Re = 2 \times 10^5$ despite the flow separation.

The values of C_l and C_d obtained in the present work for the case of $h/c = 1.0$ (negligible ground effect) are compared with the values reported in the literature [34] for NACA4412 section with no ground effect for $Re = 3.0 \times 10^6$ and a freestream turbulence level of a few hundredths of 1%, as shown in Table 2. It is interesting to see that the C_l values are comparable despite the difference in Reynolds number. Hsiun and Chen [11] from their numerical work reported an increase of about 5% in C_l for $\alpha = 5$ deg and about 4% for $\alpha = 10$ deg in the absence of ground effect when the Reynolds number was increased from 3×10^5 to 2×10^6. The values of C_d in the present work were expectedly found to be higher than the values reported in [34], which is due to the difference in Reynolds number. Hsiun and Chen [11] reported a 25% drop in C_d (from 0.0725 to 0.05) when the Reynolds number was increased from 3×10^5 to 2×10^6. Jacobs [41] indicates that variations in lift curve slope with changes in Reynolds number are very small, but in general the lift curve will be more linear as the Reynolds number increases. With increasing Reynolds number, the flow is likely to remain attached to the upper surface at higher α with the separation point very close to the trailing edge, resulting in a higher lift and lower drag. The values of drag coefficient in the present work generally increased with reducing ground clearance. The same trend is expected at higher Reynolds number also for this airfoil. A comparison of the results obtained by various researchers makes it clear that the geometry of the airfoil has a very strong influence on its characteristics in ground effect, as can be seen from the results of [6,10–12,20–24] as well as the present work. The present discussion

Table 2 Comparison of the C_l and C_d values obtained in the present work at $h/c = 1.0$ with those of Abbott and Von Doenhoff [34]

Angle of attack, α	Lift coefficient, C_l		Drag coefficient, C_d	
	Present work	Abbott and Von Doenhoff	Present work	Abbott and Von Doenhoff
0 deg	0.464	0.4	0.00798	0.00675
2 deg	0.686	0.6	0.00912	0.0069
4 deg	0.875	0.84	0.01032	0.007
6 deg	1.096	1.02	0.012	0.0083
8 deg	1.268	1.185	0.0137	0.0125
10 deg	1.362	1.33	0.0204	0.0163

reinforces the importance of the geometry of the airfoil for ground effect applications.

V. Conclusions

In the present work, a detailed investigation of the aerodynamic characteristics of NACA4412 airfoil at different angles of attack and ground clearances was carried out at $Re = 3.0 \times 10^5$ in a wind tunnel with moving ground simulation. It was found that apart from the angle of attack and the ground clearance of the airfoil, the geometry of the airfoil also has a strong influence on the aerodynamic characteristics of the configuration. The important conclusions from the present work are as follows:

1) A strong suction effect is observed on the lower surface at $h/c = 0.05$ for the angle of attack of 0 deg, due to the formation of a convergent-divergent passage between the airfoil and the ground, which led to laminar separation and a significant drop in lift force.

2) At angles of attack of 4 deg and above, high values of pressure coefficient were recorded on the lower surface at small ground clearances, with the high pressure region extending almost till the trailing edge with increasing angle of attack, which contributed to a gain in the lift force.

3) There is a loss of upper surface suction at small ground clearances for all angles of attack, contributing to a reduction in the lift force. For angles of attack up to 4 deg, this loss is higher compared to the gain on the lower surface, resulting in a lower lift close to the ground. For higher angles of 8 and 10 deg, the pressure rise on the lower surface with reducing ground clearance was considerable, resulting in a higher lift coefficient close to the ground.

4) The drag coefficient is higher close to the ground for all angles investigated mainly due to modification in the pressure distribution on the lower surface.

References

[1] Rozhdestvensky, K. V., *Aerodynamics of a Lifting System in Extreme Ground Effect*, 1st ed., Springer–Verlag, New York, 2000, p. 30.

[2] Anderson, J. D., Jr., *Fundamentals of Aerodynamics*, 3rd ed., McGraw–Hill, New York, 2001, pp. 283, 284, 334, 335, 840.

[3] Raymond, A. E., "Ground Influence on Airfoils," NACA TN-67, 1921.

[4] Reid, E. G., "A Full Scale Investigation of Ground Effect," NACA TR-265, 1927.

[5] Ollila, R. G., "Historical Review of WIG Vehicles," *Journal of Hydronautics*, Vol. 14, No. 3, 1980, pp. 65–76.

[6] Fink, M. P., and Lastinger, J. L., "Aerodynamic Characteristics of Low-Aspect-Ratio Wings in Close Proximity to the Ground," NASA TN D-926, July 1961.

[7] Staufenbiel, R. W., Haake, M., Kleineidam, G., Yeh, B. T., Weckesser, B., and Wessels, M., "Studies on the Flight Mechanics and Aerodynamics of Wing-in-Ground Effect Vehicles," Rheinish-Westfalische Technische Hochschule, Project Rept. 78/1, Aachen, Germany, 1978.

[8] Fuwa, T., Hirata, N., Hasegawa, Jun., and Hori, T., "Fundamental Study on Safety Evaluation of Wing-In-Surface Effect Ship (WISES)," *Proceedings of the Second International Conference on Fast Sea Transportation (FAST '93)*, Society of the Naval Architects of Japan, Tokyo, 1993, pp. 1257–1267.

[9] Chawla, M. D., Edwards, L. C., and Frande, M. E., "Wind-Tunnel Investigation of Wing-in-Ground Effects," *Journal of Aircraft*, Vol. 27, No. 4, 1990, pp. 289–293.

[10] Tomaru, H., and Kohama, Y., "Experiments on Wing in Ground Effect with Fixed Ground Plate," *Proceedings of the Second JSME-KSME Fluids Engineering Conference*, Japan Society of Mechanical Engineers, Tokyo, 1990, pp. 370–373.

[11] Hsiun, C. M., and Chen, C. K., "Aerodynamic Characteristics of a Two-Dimensional Airfoil with Ground Effect," *Journal of Aircraft*, Vol. 33, No. 2, 1996, pp. 386–392.

[12] Coulliette, C., and Plotkin, A., "Aerofoil Ground Effect Revisitied," *The Aeronautical Journal*, Vol. 100, No. 992, 1996, pp. 65–74.

[13] Chun, H. H., Park, I. R., and Chung, K. H., "Computational and Experimental Studies on Wings in Ground Effect and a Wig Effect Craft," *Proceedings of the Workshop on Ekranoplans and Very Fast Craft*, University of New South Wales, Sydney, Australia, 1996, pp. 38–59.

[14] Chun, H. H., Chang, C. H., Paik, K. J., and Chang, S. I., "Preliminary Design of a 20 Passenger PARWIG Craft and Construction of a 1/10 Scale Radio Controlled Model," *Proceedings of the Fourth International Conference on Fast Sea Transportation (FAST '97)*, Baird Publications, Melbourne, Australia, 1997, pp. 513–519.

[15] Akimoto, H., and Kubo, S., "Characteristics Study of Two-Dimensional Wings in Surface Effect by CFD Simulations," *Journal of the Society of the Naval Architects of Japan*, Vol. 184, 1998, pp. 47–54.

[16] Shin, M. S., "Model Test Survey Report of Wing-in-Ground Effect Ship," *Journal of Ships and Ocean Engineering*, Vol. 29, Feb. 2000, pp. 23–27.

[17] Shin, M. S., Yang, J. Y., Yang, S. H., and Wang, G. Q., "Numerical Simulation of Viscous Flow Around a Three-Dimensional Wing in Ground Effect with Endplates," *Journal of Ships and Ocean Engineering*, Vol. 29, Feb. 2000, pp. 29–39.

[18] Yang, C. J., and Shin, M. S., "Numerical Simulation of 2-D Wing-in-Ground Effect," *Transactions of the Korean Society of Computational Flows Engineering*, Vol. 3, No. 1, 1999, pp. 54–62.

[19] Ahmed, N. A., and Goonaratne, J., "Lift Augmentation of a Low-Aspect-Ratio Thick Wing in Ground Effect," *Journal of Aircraft*, Vol. 39, No. 2, 2002, pp. 381–384.

[20] Chun, H. H., and Chang, R. H., "Turbulence Flow Simulation for Wings in Ground Effect with Two Ground Conditions: Fixed and Moving Ground," *International Journal of Maritime Engineering*, Vol. 145, No. A3, 2003, pp. 1–18.

[21] Kikuchi, M., Hirano, K., Yuge, T., Iseri, K., and Kohama, Y., "Measurement of Aerofoil Characteristics by Method of Towing," *Transactions of the Japan Society of Mechanical Engineers* (in Japanese), Vol. 68, No. 676, 2002, pp. 3378–3385.

[22] Ahmed, M. R., and Sharma, S. D., "An Investigation on the Aerodynamics of a Symmetrical Airfoil in Ground Effect," *Experimental Thermal and Fluid Science*, Vol. 29, No. 6, 2005, pp. 633–647.

[23] Ahmed, M. R., "Aerodynamics of a Cambered Airfoil in Ground Effect," *International Journal of Fluid Mechanics Research*, Vol. 32, No. 2, 2005, pp. 157–183.

[24] Moon, Y. J., Oh, H. J., and Seo, J. H., "Aerodynamic Investigation of Three-Dimensional Wings in Ground Effect for Aero-Levitation Electric Vehicle," *Aerospace Science and Technology*, Vol. 9, No. 6, 2005, pp. 485–494.

[25] Ranzenbach, R., and Barlow, J. B., "Two-Dimensional Airfoil in Ground Effect, an Experimental and Computational Study," Society of Automotive Engineers Paper 94-2509, 1994.

[26] Ranzenbach, R., and Barlow, J. B., "Cambered Airfoil in Ground Effect: Wind Tunnel and Road Conditions," AIAA Paper 95-1909, 1995.

[27] Ranzenbach, R., and Barlow, J. B., "Cambered Airfoil in Ground Effect, an Experimental and Computational Study," Society of Automotive Engineers Paper 96-0909, Feb. 1996.

[28] Zhang, X., Zerihan, J., Ruhrmann, A., and Deviese, M., "Tip Vortices Generated by a Wing in Ground Effect," *Proceedings of the 11th International Symposium on Applications of Laser Techniques to Fluid Mechanics* [CD-ROM], Instituto Superior Tecnico, Lisbon, 2002.
[29] Zerihan, J., and Zhang, X., "Aerodynamics of a Single Element Wing in Ground Effect," *Journal of Aircraft*, Vol. 37, No. 6, 2000, pp. 1058–1064.
[30] Zhang, X., and Zerihan, J., "Turbulent Wake Behind a Single Element Wing in Ground Effect," *Proceedings of the 10th International Symposium on Applications of Laser Techniques to Fluid Mechanics* [CD-ROM], Instituto Superior Tecnico, Lisbon, 2000.
[31] Jasinski, W. J., and Selig, M. S., "Experimental Study of Open-Wheel Race-Car Front Wings," Society of Automotive Engineers Paper 98-3042, Nov. 1998.
[32] Ito, H., Kobayashi, R., and Kohama, Y., "The Low-Turbulence Wind Tunnel at Tohoku University," *The Aeronautical Journal*, Vol. 96, No. 954, 1992, pp. 141–151.
[33] Ahmed, M. R., Sirogane, H., and Kohama, Y., "Boundary Layer Control with a Moving Belt System for Studies on Wing-in-Ground-Effect," *JSME International Journal, Series B, Fluids and Thermal Engineering*, Vol. 42, No. 4, 1999, pp. 619–625.
[34] Abbott, I. H., and Von Doenhoff, A. E., *Theory of Wing Sections*, 1st ed., Dover, New York, 1959, Chap. 7, pp. 83, 84, 490, 491.
[35] Brendel, M., and Mueller, T. J., "Boundary-Layer Measurements on an Airfoil at Low Reynolds Numbers," *Journal of Aircraft*, Vol. 25, No. 7, 1988, 612–617.
[36] Jørgensen, F. E., *How to Measure Turbulence with Hot-Wire Anemometers—a Practical Guide*, Dantec Dynamics, Skovlunde, Denmark, 2002, pp. 32–44.
[37] Smith, A. M. O., "High-Lift Aerodynamics," *Journal of Aircraft*, Vol. 12, No. 6, 1975, pp. 501–530.
[38] Yarusevych, S., Sullivan, P. E., and Kawall, J. G., "Investigation of Airfoil Boundary Layer and Wake Development at Low Reynolds Numbers," AIAA Paper 2004-2551, June 2004.
[39] Lu, B., and Bragg, M. B., "Experimental Investigation of Airfoil Drag Measurement with Simulated Leading Edge Ice Using the Wake Survey Method," AIAA Paper 2000-3919, Aug 2000.
[40] Steinbach, D., "Comment on Aerodynamic Characteristics of a Two-Dimensional Airfoil with Ground Effect," *Journal of Aircraft*, Vol. 34, No. 3, 1997, pp. 455–456.
[41] Jacobs, E. N., "The Variation of Airfoil Section Characteristics with Reynolds Number," NACA TR-586, 1937.

A. Plotkin
Associate Editor